Modelling PID Control of a Multivariable Granular System: Continuous Fluid Analysis of a Buffer Silo

Andrei Leonard Nicusan

Process Systems & Principles of Process Control, Year 2 - Dr. Phil Robbins

School of Chemical Engineering

15.03.2019

Keywords: Multivariable, Granular fluid, PID control, Buffer silo

ABSTRACT

Buffer silos are widely used to regulate the outflow of granular fluids such as grains, flours, and different powders [1]. More complex processes such as sugar cane crushing also require the regulation of the material height in the silo [2].

This paper develops a multiloop PID control scheme for controlling the height and mass outflow in such a buffer silo that would maintain stability even in the case of severe off-measurements and real time delays. A mathematical model of the buffer silo is derived by considering the granular fluid as a continuous liquid with a discharge coefficient.

A typical weighing scale with first-order dynamics is used to measure the mass outflow. A method of inferring the fluid height is successfully developed using a zero-order approximation of the weighing scale to predict and control the height.

A Simulink™block model of the control system is used to analyse the closed-loop response of the system and the height-inferring method. Overall, the control system proved very robust in handling disturbances, real time delays and off-measurements.

CONTENTS

1 INTRODUCTION

Buffer silos (or hopper silos) are widely used in series to regulate the outflow of a granular fluid from a bigger storage silo in a manner depicted in Figure 1. They are used in the food industry to transport ingredients such as flours, starches, semolina and different powders to the production line [1]. Equivalent buffer systems are used in more complex processes, such as sugar cane crushing, in which also maintaining a steady height is essential [2].

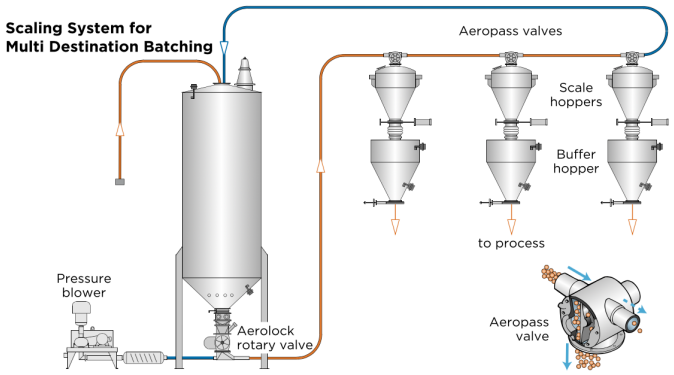

Figure 1. Example of buffer silos (hopper silos) being used in series to regulate the mass outflow of bakery ingredients (Copyright Coperion 2019 [1])

Such systems pose a variety of problems from a control perspective: granular fluids are compressible, leading to possible off-measurements of the mass outflow. A weighing scale for the mass outflow can be placed further away from the buffer silo, introducing real time-delay in the system, which can destabilise it greatly. Moreover, the control system should also be economical: sophisticated sensors such as acoustic phased-array antennas for height-measurement can be costly.

The aim of this paper is to develop a control system for the mass outflow and granular fluid height in such a buffer silo. The main objectives for the control system are:

1. The system should be stable even in the case of severe off-measurements and real time delay.
2. The implementation should be economical, avoiding sophisticated equipment.

First, an analytic model of the buffer silo will be developed, treating the granular fluid as a liquid with a discharge coefficient.

It was recognised that the outflow velocity is driven by the potential energy of the granular fluid inside the silo. This creates the possibility of

inferring the fluid height from the mass outflow. A method to do this will be developed, **reducing the number of sensors needed to one**: a typical weighing scale.

Two PID controllers will be placed in a multiloop arrangement with 1-1/2-2 coupling. They will be tuned empirically, using the characteristic equation of the developed closed-loop transfer function and Nyquist diagrams. The system response and stability will then be analysed for disturbances, step-changes in the controlled variables, increasing real time-delay and off-measurements. The height-inferring system response will also be analysed.

2 MATHEMATICAL MODELLING OF THE BUFFER SILO

2.1 Control Problem Setup

The buffer silo will be modelled as a cylindrical tank of inner area A_T connected to an upper grain transport pipe. A diverter valve splits the top mass inflow $\dot{m}_T(kg/s)$, directing $\dot{m}_i(kg/s)$ into the silo and diverting $\dot{m}_D(kg/s)$ to the next silos. Therefore:

$$\dot{m}_i = \dot{m}_T - \dot{m}_D \tag{1}$$

The maximum limit of the diverted mass inflow $\dot{m}_D(kg/s)$ is, naturally, the top mass inflow $\dot{m}_T(kg/s)$.

The granular fluid height is $h(m)$, while the silo height is $H(m)$.

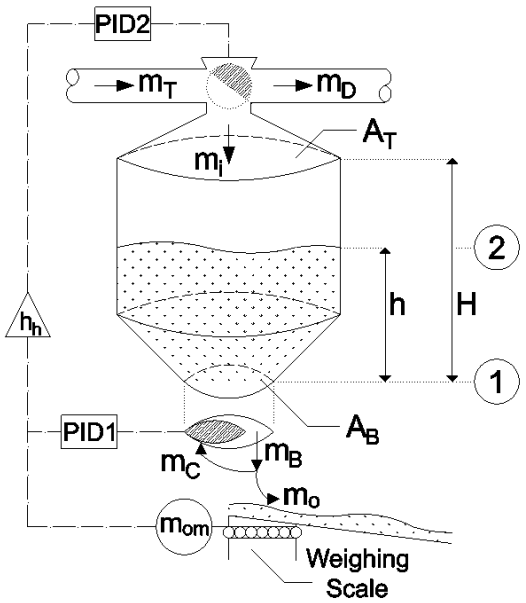

Figure 2. Simplified diagram of the buffer silo

At the bottom of the silo, a chute with variable angle regulates the outlet area and, consequently, the mass outflow. When the chute is fully open, the outlet area at the bottom of the tank is A_B. Associated with this area is the maximum mass outflow at the bottom of the silo $\dot{m}_B(kg/s)$:

$$\dot{m}_B = C_D \rho A_B u_o \tag{2}$$

Where C_D is a non-dimensional discharge coefficient, $\rho(kg/m^3)$ is the granular fluid's density and $u_o(m/s)$ is the outflow velocity.

The chute decreases the outlet area, and so it decreases the mass outflow by $\dot{m}_C(kg/s)$, leaving a mass outflow of $\dot{m}_o(kg/s)$. It is assumed that the chute decreases the outflow linearly. Therefore:

$$\dot{m}_o = \dot{m}_B - \dot{m}_C \tag{3}$$

The maximum limit of the mass outflow stopped by the chute $\dot{m}_C(kg/s)$ is, naturally, the maximum mass outflow at the bottom of the silo $\dot{m}_B(kg/s)$.

As the silo outflow velocity is only driven by the potential energy of the granular fluid, the fluid height can be inferred from the mass outflow. This model aims to control the fluid height h and mass outflow m_o by only measuring the mass outflow.

The key parameters for this control problem are summarised in Table 1.

Table 1. Key parameters of this paper's control problem

Controlled variables	$\dot{m}_o, \quad h$
Manipulated variables	$\dot{m}_c, \quad \dot{m}_D$
Measured variables	$\dot{m}_o$
Disturbance variables	$\dot{m}_T$

2.2 Process Mathematical Derivation

The aim of this subsection is to find a mathematical law which relates the controlled variables to the manipulated and disturbance variables. Written in matrix form, the sought equation is of the form:

$$\begin{bmatrix} \dot{m}_o(t) \\ h(t) \end{bmatrix} = \begin{bmatrix} M_{11} & M_{12} \\ M_{21} & M_{22} \end{bmatrix} \begin{bmatrix} \dot{m}_c \\ \dot{m}_d \end{bmatrix} + \begin{bmatrix} M_3 \\ M_4 \end{bmatrix} \dot{m}_T \tag{4}$$

2.2.1 Energy Balance Using Bernoulli's equation, conducting an energy balance between points (1) and (2) as shown in Figure 2, yields:

$$P_1 + \frac{\rho u_1^2}{2} + \rho g z_1 = P_2 + \frac{\rho u_2^2}{2} + \rho g z_2 \tag{5}$$

Assuming that both the outlet and top of the granular fluid are at atmospheric pressures, then $P_1 = P_2$. Taking point (1) as the datum, then $z_2 - z_1 = h$. The velocity of the top of the granular fluid is $u_2 = \frac{dh}{dt}$. It is assumed that the change in height is small and slow. As such, when squared, the fluid top velocity u_2 is small enough to be neglected. Therefore:

$$u_o = u_1 = \sqrt{2gh} \tag{6}$$

Combining Equations 2 and 6 correlates the mass outflow with the fluid's height:

$$\dot{m}_B = C_D \rho A_B \sqrt{2gh} \tag{7}$$

This control problem will be solved in the Laplace space (s domain), using linear differential equations. As this problem is concerned with small changes in h, Equation 7 can be linearised using Taylor Approximation around a fixed (Steady-State) height h_s:

$$\begin{aligned}\dot{m_B} =& C_D\rho A_B\sqrt{2g}\left[\sqrt{h_s} + \frac{1}{2\sqrt{h_s}}(h - h_s)\right] \\ =& \left[C_D\rho A_B\sqrt{2g}\left(\sqrt{h_s} - \frac{h_s}{2\sqrt{h_s}}\right)\right] + \\ & \left[C_D\rho A_B\sqrt{2g}\frac{1}{2\sqrt{h_s}}\right]h \\ \implies & \dot{m_B} = \alpha + \beta h\end{aligned} \tag{8}$$

Where α and β are constants particular to a given system. Based on Equation 8, their dimensions are kg/s and $(kg/s)/m$, respectively.

2.2.2 Mass Balance Conducting an unsteady-state mass balance around the silo yields:

$$\dot{m_i} = \dot{m_o} + \rho\frac{dV}{dt} = \dot{m_o} + \rho A_T\frac{dh}{dt} \tag{9}$$

Note: it is assumed that the variance in fluid height happens in the straight-walled section of the silo. Therefore, even if the lower side of the silo is angled, the variance in volume happens linearly with height.

2.2.3 Deviation Variables This control problem is concerned with changes to the controlled variables relative to Steady-State values. Therefore, it would be helpful to rewrite Equations characterising the system in terms of the deviation from a Steady-State (X_s, where X is a generic variable) value. At Steady-State, Equations 10 are true:

$$\begin{cases}\dot{m_{is}} = \dot{m_{os}} \\ \dot{m_{is}} = \dot{m_{Ts}} - \dot{m_{Ds}} \\ \dot{m_{os}} = \dot{m_{Bs}} - \dot{m_{Cs}} \\ \dot{m_{Bs}} = \alpha + \beta h_s\end{cases} \tag{10}$$

Subtracting Equations 10 from Equations 9, 1, 3 and 8, respectively, and using the star-notation for the deviation variables ($X^* = X - X_s$, where X is a generic variable), yields Equations 11:

$$\begin{cases}\dot{m_i}^* = \dot{m_o}^* + \rho A_T\frac{dh^*}{dt} \\ \dot{m_i}^* = \dot{m_T}^* - \dot{m_D}^* \\ \dot{m_o}^* = \dot{m_B}^* - \dot{m_C}^* = \beta h^* - \dot{m_C}^*\end{cases} \tag{11}$$

Note: $dh^* = d(h - h_s) = dh$, as h_s is a constant.

2.2.4 Manipulation in the Laplace domain Laplace transforms are very helpful in control problems, as they reduce solving linear differential equations to simple algebraic manipulation. Equations 11 can be rewritten in the Laplace domain as:

$$\begin{cases}M_i^*(s) = M_o^*(s) + \rho A_T(sH^*(s) - h^*(0)) \\ M_i^*(s) = M_T^*(s) - M_D^*(s) \\ M_o^*(s) = \beta H^*(s) - M_C^*(s)\end{cases} \tag{12}$$

For this control problem, any disturbances are considered to take place after $t > 0$. As such, at $t = 0$, the system is at Steady-State, implying $h = h_s$. Therefore, $h^*(0) = 0$.

Substitution of the second and third equations of (12) into the first and algebraic manipulation yield an expression for $H^*(s)$:

$$\begin{aligned}(M_T^*(s) - M_D^*(s)) &= (\beta H^*(s) - M_C^*(s)) + \rho A_T(sH^*(s)) \\ \implies H^*(s) &= \frac{M_C^*(s) - M_D^*(s) + M_T^*(s)}{\rho A_T s + \beta}\end{aligned} \tag{13}$$

Substituting Equation 13 into the third equation of (12) yields an expression for $M_o^*(s)$:

$$\begin{aligned}M_o^*(s) &= \beta\frac{M_C^*(s) - M_D^*(s) + M_T^*(s)}{\rho A_T s + \beta} - M_C^*(s) \\ \implies M_o^*(s) &= \frac{-\rho A_T s M_C^*(s) - \beta M_D^*(s) + \beta M_T^*(s)}{\rho A_T s + \beta}\end{aligned} \tag{14}$$

Dividing Equations 13 and 14 by β and using the notations $\tau_P = \frac{\rho A_T}{\beta}$ with units $\frac{kg/m^3m^2}{kg/s/m} = s$, and $\frac{1}{\beta} = K_P(\frac{m}{kg/s})$, they can be written in matrix form as:

$$\begin{aligned}\begin{bmatrix}M_o^*(s) \\ H^*(s)\end{bmatrix} &= \begin{bmatrix}\frac{-\tau_P s}{\tau_P s+1} & \frac{-1}{\tau_P s+1} \\ \frac{K_P}{\tau_P s+1} & \frac{-K_P}{\tau_P s+1}\end{bmatrix}\begin{bmatrix}M_c^*(s) \\ M_d^*(s)\end{bmatrix} + \begin{bmatrix}\frac{1}{\tau_P s+1} \\ \frac{K_P}{\tau_P+1}\end{bmatrix}M_T^*(s) \\ \Leftrightarrow \begin{bmatrix}M_o^*(s) \\ H^*(s)\end{bmatrix} &= \begin{bmatrix}\frac{-\tau_P s}{\tau_P s+1} & \frac{-1}{\tau_P s+1} & \frac{1}{\tau_P s+1} \\ \frac{K_P}{\tau_P s+1} & \frac{-K_P}{\tau_P s+1} & \frac{K_P}{\tau_P+1}\end{bmatrix}\begin{bmatrix}M_c^*(s) \\ M_d^*(s) \\ M_T^*(s)\end{bmatrix}\end{aligned} \tag{15}$$

This is the required multivariable process equation which will be used to model the system response in Simulink™in the following sections.

2.3 Feedback Loop Derivation

This subsection aims to create a mathematical model of the measurement system and derive the expression correlating the measured mass outflow with the granular fluid height.

2.3.1 Measurement system The mass outflow will be measured by a weighing scale underneath the chute opening of the silo. The scale will be modelled as having a first-order response:

$$\tau_m\frac{dm_{om}}{dt} + m_{om} = K_m\dot{m_o} \tag{16}$$

Where K_m is the gain of the measurement system (units $mA/(kg/s)$), transforming a given mass outflow $\dot{m_o}(kg/s)$ into an electric signal $m_{om}(mA)$.

At Steady-State, $m_{oms} = K_m\dot{m_{os}}$. Subtracting this from Equation 16 to rewrite it in terms of deviation variables, then taking the Laplace transforms yields:

$$M_{om}^*(s) = \frac{K_m}{\tau_m s + 1}M_o^*(s) \tag{17}$$

2.3.2 Inferring fluid height In a real system, only electrical signals are known. As such, to infer the fluid height from the mass outflow, an expression needs to be derived correlating the fluid height $h(m)$ with the signals from the measurement ($m_{om}(mA)$) and control (PID controllers) systems.

Derivation will be conducted in the Laplace domain. Based on Equation 12, the height deviation of the fluid is:

$$H^*(s) = \frac{M_o^*(s) + M_C^*(s)}{\beta} \tag{18}$$

This relation has to be rewritten in terms of known electrical signals. The weighing scale transforms the mass outflow $M_o^*(s)$ into an electrical

signal $M^*_{om}(s)$ according to Equation 17. However, for sensors of order greater or equal to 1, transforming an electrical signal back into the physical quantity is not possible. In the Laplace domain, such a transformation would imply a Transfer Function with the numerator having a higher order than the denominator: $M^*_o(s) = \frac{\tau_m s+1}{K_m} M^*_{om}(s)$. Causality is axiomatic in the physical world, and such an operation would imply knowledge of the future, rendering this approach unfeasible.

However, for inferring the fluid height, the sensor's response can be approximated as zero order:

$$M^*_o(s) \approx M^*_{oh}(s) = \frac{1}{K_m} M^*_{om}(s) \tag{19}$$

This implies ignoring the sensor's dynamics and only considering its response as static. The physical meaning of this is that, for every given $M_{om}*$, M_{oh} is the associated mass outflow **if the system was at Steady-State**.

At steady values, the inferred M^*_{oh} will be equal to M^*_o. During changes in the system variables, the inferred M^*_{oh} will 'hunt' the real M^*_o, following it. This associated error will be quantified in the following sections, based on the Simulink™model.

The deviation in the mass outflow stopped by the chute position M^*_C is dictated by the position of the chute. This is the final control element (FCE) that is manipulated by the PID controller's electrical response. The same zero-order approximation as before can be made on it:

$$M^*_C(s) \approx M^*_{Ch}(s) = K_{Chute} \times K_{ep} \times Z_{PID} \tag{20}$$

Where M^*_{Ch} is the inferred mass outflow stopped by the chute, $K_{Chute}(kg/s/psi)$ is the gain of the chute (the ratio of the Steady-State mass output and pneumatic input), $K_{ep}(psi/mA)$ is the electronic-pneumatic transducer gain, and $Z_{PID}(mA)$ is the electrical signal from the PID controller.

Therefore, the inferred deviation in fluid height H^*_h is:

$$H^*(s) \approx H^*_h(s) = \frac{1}{\beta}\left(\frac{1}{K_m} M^*_{om}(s) + K_{Chute} K_{ep} Z_{PID}\right) \tag{21}$$

3 SIMULINK™MODEL ANALYSIS

3.1 Model and Numerical Values

Based on the equations developed in Section 2, a Simulink™model can be developed. For further analysis, the particular values depicted in Table 2 were used.

For this system, the mass outflow M^*_o is, naturally, strongly-coupled to the chute response. A 1-1/2-2 multiloop coupling method is used: the chute is manipulated to control the mass outflow, leaving the diverter valve to be manipulated to control the fluid height.

Note that in Figure 3 the manipulated variables' response is inverted relative to the controller input: if the setpoint is higher than the measured variable, then more mass should be diverted or stopped. Therefore, each error signal output has the minus (-) and plus (+) signs inverted in the block model.

3.2 Stability Analysis

3.2.1 Characteristic equation For the analytical stability analysis, the closed loop transfer function will be derived. For this, no dead time was considered. Any time delay in the measurement system was neglected: for this subsection, the weighing scale works ideally.

Written in matrix form, the closed loop transfer function is:

Table 2. Numerical values for the simulation of the buffer silo

System	Parameter	Value	Units
Buffer Silo	ρ	700	kg/m^3
	A_T	4	m^2
	A_B	0.05	m^2
	β	46.5	$(kg/s)/m$
Process	K_p	0.0215	$m/(kg/s)$
	τ_p	60.2	s
Measurement System	K_m	0.185	$mA/(kg/s)$
	τ_m	0.5	s
	K_h	1.4	mA/m
Chute	K_{ep1}	2	psi/mA
	K_C	2	$(kg/s)/psi$
	τ_C	25	s
Diverter Valve	K_{ep2}	2	psi/mA
	K_D	8	$(kg/s)/psi$
	τ_D	25	s

$$\begin{aligned} Y &= [PID]K_{ep}[FCE]G_P\left(G_m Y - K_m Y_{set}\right) \\ \Leftrightarrow Y &= \left[I_2 - [PID]K_{ep}[FCE]G_P G_m\right]^{-1} \\ &\quad [PID]K_{ep}[FCE]G_P G_m K_m Y_{set} \end{aligned} \tag{22}$$

Where:

- Y (2×1) is a **column vector** of the controlled variables (namely $M^*_o(s)$ and $H^*(s)$).
- Y_{set} (2×1) is a **column vector** of the set points of the controlled variables.
- $[PID]$ (2×2) is a **diagonal matrix** of the PID controllers' response.
- K_{ep} (2×2) is a **diagonal matrix** of the electronic-pneumatic transducers' gains.
- $[FCE]$ (2×2) is a **diagonal matrix** of the Final Control Elements (namely the chute and the diverter valve, respectively) transfer functions.
- G_P (2×2) is a **square matrix** of the 4 process transfer functions.
- K_m (2×2) is a **diagonal matrix** of the measurement gains.
- G_m (2×2) is a **diagonal matrix** of the measurements' transfer functions.

Note: because of the non-standard nature of the height inferring system, typical block diagram algebra cannot be done. As such, for the purpose of stability analysis, the measured height is treated as if it were measured by a different sensor with the same time constant τ_m as the weighing scale.

Therefore, the characteristic equation is:

$$det\left(I_2 - [PID]K_{ep}[FCE]G_P G_m\right) = 0 \tag{23}$$

Equation 23 is written explicitly for this particular model in the Appendix.

The characteristic equation is used to asses a control system's stability. If the complex roots of the characteristic equation are on the left-hand plane (that is, the real part is negative), then any bounded input will have a bounded output- hence the system will have a stable response [3].

3.2.2 PI gains stability margins Generally, a PID controller's response in the Laplace domain takes the form:

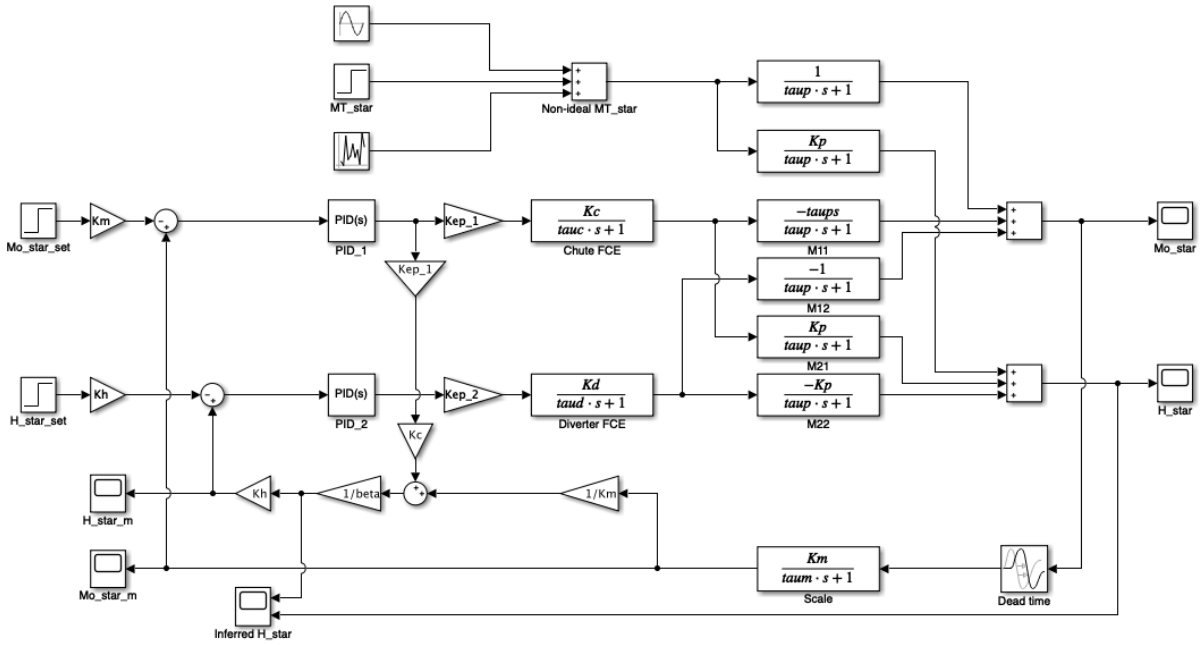

Figure 3. Simulink™block diagram model of the buffer silo control system

$$[PIDResponse] = K_{cp} + \frac{K_{ci}}{s} + K_{cd}s \tag{24}$$

For assessing the stability region of the PID controller gains, their normalised values were used according to Equation 25. As the integral term is known to introduce instability in the system, the stability region of the proportional gains was also evaluated for a unity normalised integral gain for both controllers.

$$\begin{aligned} \overline{K_{cp}} &= K_{cp}K_{ep}K_{FCE} \\ \overline{K_{ci}} &= K_{ci}K_{ep}K_{FCE} \\ \overline{K_{cd}} &= K_{cd}K_{ep}K_{FCE} \end{aligned} \tag{25}$$

The stability region of the 2 controller proportional gains was evaluated at discrete points of the varying K_{cp1} and K_{cp2}. The system is considered stable if **all** the complex solutions of the characteristic equation (23) are in the left plane.

The region shown in Figure 4 qualitatively follows the expected stability curve of a TITO system (Seborg et al., 2016, Chapter 18 [3]). The figure also shows that a unity normalised integral gain in both controllers introduces instability for low proportional gains of controller 2. It seems that the stability of the system is mostly regulated by controller 2, as it is stable for most controller 1 proportional gains. This can be further evaluated using Nyquist diagrams for varying proportional gains.

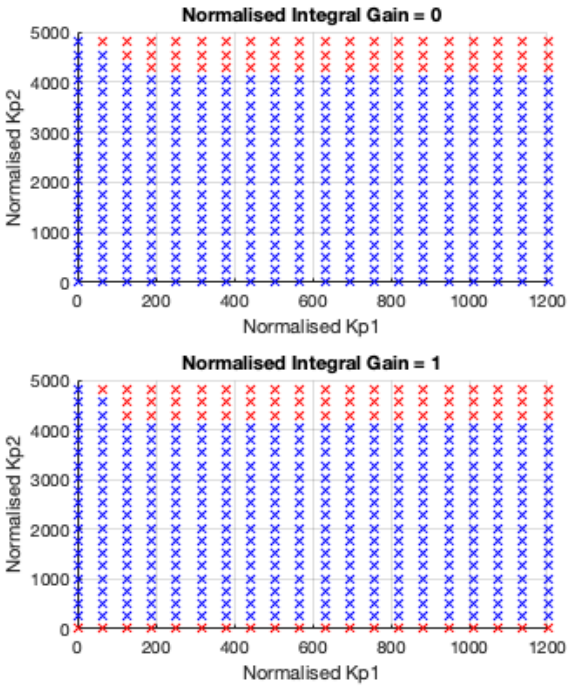

Figure 4. The stability region of the 2 controllers' proportional gains. In blue is a stable system; in red is an unstable system. The actual proportional gains for this system are varied between 0.01 and 300 (mA/mA)

3.2.3 Nyquist diagrams Nyquist diagrams can be used to provide insight into how close a system is to instability [3]. Their graphs will be analysed for increasing proportional gains, for each controller.

Two different runs will be conducted:

1. Varying controller 1 parameters:
   - Controller 1 gains will be 800, then 1600.
   - Controller 2 gain will be set to 3200.
   - The system is stable in both cases.
2. Varying controller 2 parameters:
   - Controller 1 gain will be set to 800.

- Controller 2 gain will be 3200, then 6400.
- The system is unstable for $K_{cp2} = 6400$, as shown in Figure 4.

As shown in Figure 5, when varying the proportional gain K_{cp1} of controller 1, the response of the mass outflow M_o^* does not get any closer to the critical point $(-1+0j)$. Doubling the proportional gain only yields a larger circle with the same distance on the real axis from the critical point.

In the response of the variance in fluid height H^*, the critical point is already encircled. This seems invariant to the increase in the proportional gain.

Therefore, for a stable K_{cp2}, any increase in the proportional gain K_{cp1} of controller 1 should not destabilise the system.

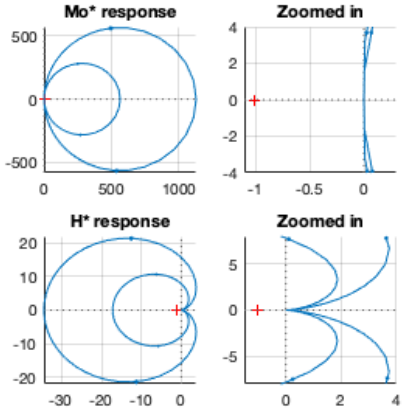

Figure 5. Nyquist diagram for varying the proportional gain K_{cp1} of controller 1. The x- and y-axes represent the real- and imaginary-axes, respectively. The critical point $(-1 + 0j)$ is shown as a red cross.

However, when increasing the proportional gain K_{cp2} of controller 2, the system can become unstable. This can be attributed to the fact that the graphs in Figure 6 get closer to the critical point $(-1 + 0j)$.

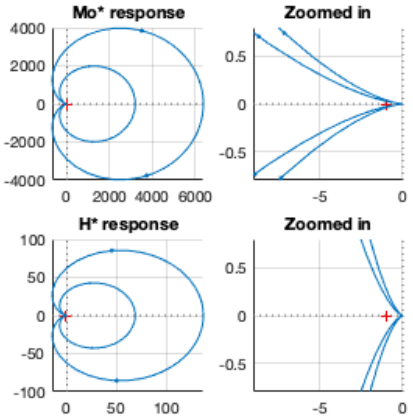

Figure 6. Nyquist diagram for varying the proportional gain K_{cp2} of controller 2. The x- and y-axes represent the real- and imaginary-axes, respectively. The critical point $(-1 + 0j)$ is shown as a red cross.

Therefore, controller 2 should be tuned first, as it is the one that mainly introduces instability in the system.

3.3 PID Controllers Tuning

The two PID controllers will be manually tuned using the Simulink ™block model response. As the system is expected to work even in the case of severe off-readings and real dead time, stability is essential.

The main objectives when tuning the controllers are, in the order of priority, as follows:

1. Overall system stability.
2. Speed of the mass outflow M_o^* response.
3. Speed of the height H^* response.

The order of tuning is based on the analysis conducted in the previous subsections: initially, all normalised gains are set to unity. Controller 2 is tuned first for the proportional gain K_{cp2}, then integral gain K_{ci2}, taking care of the instability that may be induced. Once a stable setting has been reached, controller 1 is tuned for the speed of response. The derivative gains K_{cd1} and K_{cd2} are finally tuned to improve stability. Several iterations of this are done to heuristically tune the controllers for the best stability and for good speed of response.

The empirical tuning parameters found for a system with a real measurement time delay of $10s$ are depicted in Table 3.

Table 3. Proportional, Integral and Derivative gains of the two controllers

	PID1 normalised	**PID2** normalised	**PID1** actual	**PID2** actual
K_{cp}	8.8	112	2.2	7
K_{ci}	2.6	1.6	0.065	0.1
K_{cd}	60	224	15	14

It can be noted that the normalised values are several orders of magnitude smaller than what is shown in the stability region in Figure 4. This is due to the fact that real dead time delay cannot be considered when analytically computing the roots of the characteristic equation, as it would give infinite solutions [CITE SEBORG?]. The computed stability region (Figure 4) and Nyquist diagrams (Figures 5 and 6) were used to gain an intuition of the effect on stability of increasing proportional gains.

3.4 Dimensionless Variables

It is expected that the system variables scale with the process parameters they are multiplied with. Therefore, defining some dimensionless variables will give more insight into the response of the buffer silo:

$$\begin{cases} \text{Dimensionless time} = & \frac{t}{\tau_P} \rightarrow \frac{s}{s} \\ \text{Dimensionless mass outflow} = & \frac{m_o^*}{M} \rightarrow \frac{kg/s}{kg/s} \\ \text{Dimensionless height} = & \frac{h^*}{K_p M} \rightarrow \frac{m}{m/(kg/s)kg/s} \end{cases} \tag{26}$$

Where M is the magnitude of the step-change of either M_T^* or M_{oset}^*, depending on which one is defined as non-zero.

3.5 Open-loop Response

The open-loop response of the system is depicted in Figure 7. For changes in the top mass inflow M_T, the buffer silo shows the expected self-regulating nature.

For the step-change of unity magnitude, the system has a typical first-order response. This is expected, as shown in the process equation (15).

For the sinusoidal input of unity amplitude and frequency 0.08, the system exhibits some natural disturbance regulation, as it "compresses" the unity amplitude of the top mass inflow 5-fold, resulting in a variance of amplitude 0.2 in m_o^* and h^*.

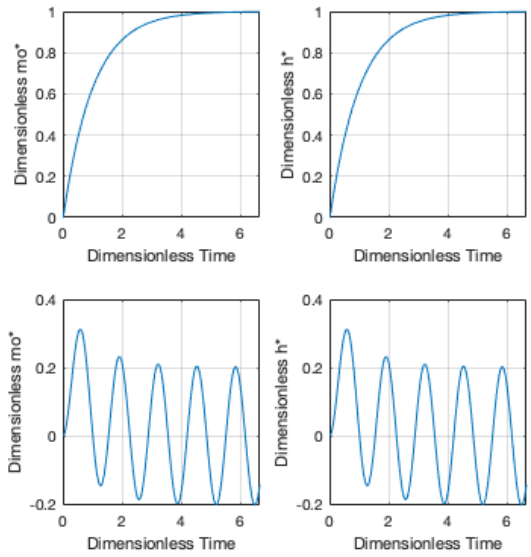

Figure 7. Open-loop response of the system for disturbance M_T: step-change of 1 (top) and sinusoidal input of amplitude 1 and frequency 0.08 (bottom)

3.6 Closed-loop Response

The response of the system with the two PID controllers engaged will be analysed in this subsection. The PID parameters used are the ones depicted in Table 3. For every paragraph the measurement time delay is unity, besides "Time delay analysis".

3.6.1 Disturbance response The closed-loop response of the system for changes in the top mass inflow M_T is depicted in Figure 8.

For the step-change of unity magnitude in the top mass inflow M_T, the rise time in the mass outflow response is 0.0009 $(0.05s)$ and 0.55 $(33s)$ for the height.

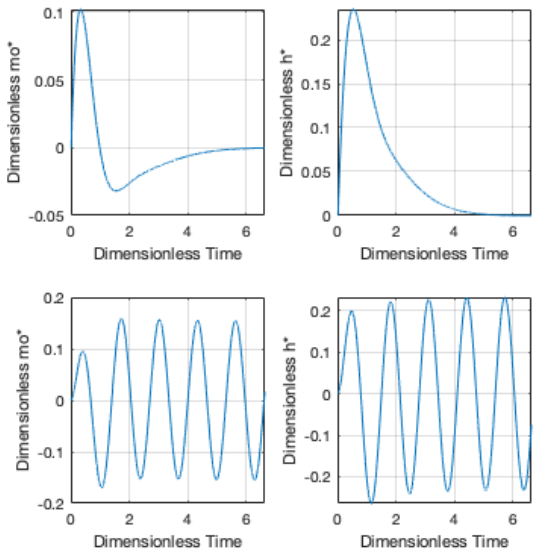

Figure 8. Closed-loop response of the system for disturbance M_T: step-change of 1 (top) and sinusoidal input of amplitude 1 and frequency 0.08 (bottom)

The settling time of the system is 5 ($\approx 300s$) for m_o^* and 4 ($\approx 240s$) for h^*.

The peak of m_o^* is 0.1, showing a 10-fold reduction from the open-loop response. The peak of h^* is 0.25, exhibiting a 4-fold reduction.

After the peak has been reached, the mass outflow response has an undershoot, while the height decreases steadily to the set value. This shows a faster, more aggressive setting of PID1.

However, for the sinusoidal input, the reduction in amplitude is only 18% for the mass outflow. The height has an initial peak decrease, but stabilises at an amplitude that is 10% larger than the open-loop response. This may seem problematic, but the actual amplitude of h^* is $0.0043m$, which is insignificant compared to the height of a real silo.

The response of the mass outflow is much quicker, as m_o is very strongly coupled with the chute position and the controllers were tuned with this in mind.

3.6.2 Step-change response The closed-loop response of the system for step-changes in the controlled variables' m_o^* (top) and h^* (bottom) step-points is depicted in Figure 9.

For the step-change in the set mass outflow m_{oset}^*, m_o^* exhibits a rise time of 1.37 ($\approx$ $82s$), while the height h^* takes a very short time of 0.0051 ($\approx 0.3s$).

After the initial rise, the mass outflow m_o^* plateaus at 0.88 ($=$ $0.88kg/s$), then slowly approaches the set point, without any overshoot. Even though its rise time was very short, the settling time is almost double at 2.4 ($\approx$ $144s$). The mass outflow has a very robust transient behaviour.

The height h^* reaches a peak of 0.23 ($=$ $0.005m$), before it undershoots; it then approaches the set value, giving a settling time of 5.26 ($\approx 316s$). However, the actual variance in height is of the order of millimetres, which is insignificant compared to the height of the silo.

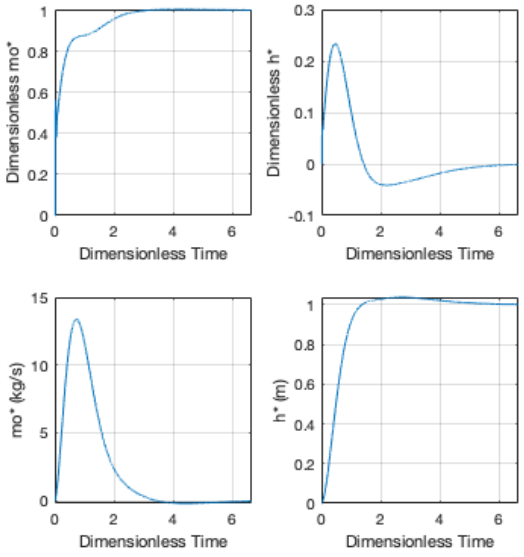

Figure 9. Closed-loop response of the system for unity step changes of controlled variables' set points: m_o^* (top) and h^* (bottom)

For the step-change in the set height h_{set}^*, the height h^* has a rise time of 0.8 ($\approx 48s$), while the mass outflow m_o^* takes 0.09 ($\approx 5.4s$).

After the initial rise, the height h^* has a small overshoot of 3%, before it slowly decreases to the set point. Even though the rise time was quite short, the settling time is almost quadruple at 4 ($\approx 241s$). However, the

overshoot is of the order of millimetres, rendering the response in height quite quick and robust.

However, the mass outflow m_o^* varies significantly, showing a peak of $13.4kg/s$, before quickly decreasing back to the set point. The settling time is 3 ($\approx 180s$). It should be noted that this is still 3.5 times less than the maximum mass outflow for a system which has a fluid height of $1m$. Therefore, the limit of the mass stopped by the chute is still not reached.

The system response in changes in the controlled variables' set point shows that the mass outflow can very easily be regulated using the chute. However, the height is much harder to control using the diverter valve, inducing greater fluctuations in the mass outflow. Overall, the system response is very robust, usually not showing large overshoots or hunting.

3.6.3 Effect of real time delay In real applications, the weighing scale can be further away from the buffer silo, introducing real time delay in the measurement of the mass outflow $\dot{m}_o$. This can greatly destabilise the system: even a time delay of $1s$ forces the use of controller proportional gains that are even 100 times smaller than the ideal case (as shown in Figure 4).

The response of the system for a step change in disturbance M_T^* for different time delays is depicted in Figure 10.

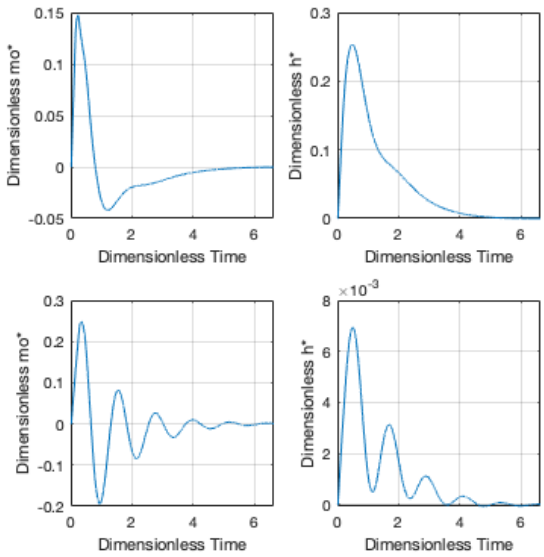

Figure 10. Closed-loop response of the system against a unity step change in disturbance M_T^* for varying real time delay in the measurement system: $8s$ (top) and $16s$ (bottom)

For a real time delay of $8s$, the rise and settling times are approximately the same as for $1s$ (graph in Figure 8). However, the peak has increased by 50% for the mass outflow m_o^* to 0.15 ($= 0.15kg/s$), while remaining the same for the height h^*. The shape of the graph only differs slightly from the $1s$ time delay system: the plateaus are reached more abruptly.

For a real time delay of $16s$, the system is clearly getting closer to instability: the responses of the controlled variables do not plateau steadily anymore, as they start oscillating. The rise and settling times remain approximately the same as for the other time delays.

The peak has increased even more to 0.25 ($= 0.25kg/s$) for the mass outflow. The height peaks at 0.007 ($\approx 0.00015m$), which is 3.5 times smaller than for the systems with smaller time delays. This may indicate that for increasing time delays, the effect of controller 2 becomes more apparent than that of controller 1, leading to a less stable system, a more aggressive response in height, and worse disturbance rejection in the mass outflow.

The real time delay of the measurement system is usually fixed due to physical constraints such as sensor position relative to the process [3]. Therefore, when tuning the controllers of a real buffer silo, the real time delay can more easily be taken into account. For better stability in the case of larger real time delays, the tuning should start with a lower integral gain of controller 2, then vary the proportional and derivative gains accordingly.

3.6.4 Height inferring system The response of the inferred height h_h compared to the actual height h for step, sinusoidal and noise disturbance is depicted in Figure 11. It is clear that the inferred height successfully follows the real height.

The height-inferring system will also be compared to the response of an equivalent model that uses a separate measurement of the height with the same time constant as the weighing scale. The responses are depicted in Figure 12.

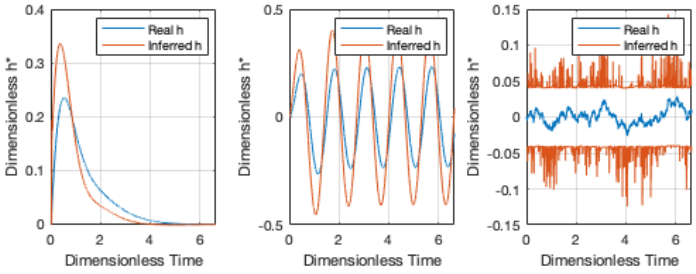

Figure 11. Reponse of the inferred height h_h compared to the actual height h for step (left), sinusoidal (center) and noise (right) changes of unity magnitude in the disturbance M_T. The graph for the noise was cut for clarity.

For the step-change, the inferred height reaches a peak of 0.33 that is 1.4 times bigger than the real height's peak of 0.24. When decreasing, the inferred height slightly underpredicts the real height before reaching the same steady value. The settling time is the same for both.

For the sinusoidal disturbance M_T, the inferred height follows the real height with a relatively small delay of 0.09 ($\approx 5.5s$). The amplitude of the inferred height of 0.45 ($\approx 0.01m$) is 1.7 times larger than the amplitude of the real height at 0.26 ($\approx 0.006m$).

However, for a disturbance M_T of noise of maximum amplitude of unity, the inferred height has a relatively large error associated that can reach even 800%. Qualitatively, the inferred height follows the response of the real height.

The zero-order approximation of the measurement system leads to an inferred height that successfully follows the real height, with relatively small delay and error. Problems may arise for very noisy measurements, as the associated error can be large relative to the real height. However, the actual variance in height is of the order of millimetres. Therefore, even for an error of 800%, the variance in the inferred height would be of the order of centimetres- which is still insignificant compared to the size of a real silo.

Overall, the height-inferring system can successfully be used to predict and control the real height.

3.6.5 Separate height measurement comparison The equivalent system with another measurement for the height with the same time constant as the weighing scale exhibits lower associated error and better following of the real height. The delay between the disturbances is also decreased.

The biggest advantage of the separate height measurement system is clear in the case of noisy disturbances: the associated error is no longer 8-fold as for the inferred-height system. The measured height follows the real one very closely.

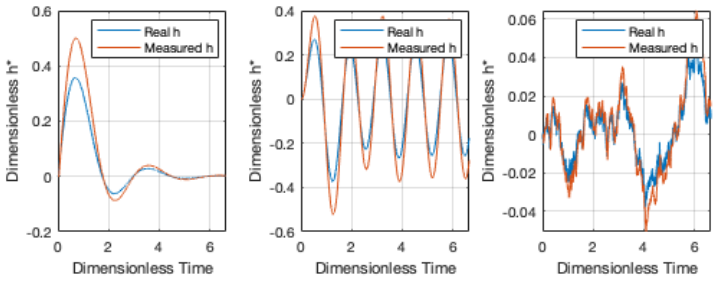

Figure 12. Reponse of the inferred height h_h compared to the actual height h for step (left), sinusoidal (center) and noise (right) changes of unity magnitude in the disturbance M_T. Note this for the equivalent system with another measurement for the height with the same time constant as the weighing scale.

However, the most important thing to note is that, for the same controllers settings and measurement time delay, **the system gets closer to instability**. The response starts exhibiting oscillations. This may be attributed to an increased response in controller 2, which is the one that mainly introduces instability in the system. Different PID tunings and further comparison of the two height measurement techniques can be the scope of another study.

3.6.6 Off-measurements Granular fluids in some storage silos can exhibit severe compression of up to 22% for pressures of $15kPa$ [4]. This can pose problems in the case of silos in general, as the density of the outflow (the one that is measured) will be different than that of the granular fluid in the silo, especially at the bottom of it, where the pressure can be high. For a system with a fluid height of $h = 1m$ and density $\rho = 700kg/m^3$, the pressure at the bottom would be $P = \rho gh = 6.9kPa$.

For this analysis, the real mass outflow is multiplied by a constant of 0.8 before being measured, depicting the case of 20% off measurements of M^*_{om}. The response of the system is depicted in Figure 13.

For a unity step-change in the disturbance (the top mass inflow M_T), the response of the system is the same as for accurate measurements (Figure 8). The mass outflow and height both return to zero error.

The error in the settled value becomes apparent in the case of a unity step-change in the set mass outflow M^*_o. The mass outflow settles at a value of 1.25, 25% off from the set-point of 1. The height settles at a value of 0.25 ($\approx 0.005m$), not returning to the set-point of zero. Qualitatively, the graphs follow the same curve as in Figure 8 for accurate measurements.

A measurement that is 20% off leads to an increase of 0.25 in both the mass outflow and height. This is not significant for the height, as the error is still in the order of millimetres. However, the mass outflow is 25% off from the required set point, which may be problematic in some circumstances.

It is very important to note that the stability of the system does not seem to be affected by off-measurements, as the rise and settling times of the controlled variables are the same as for accurate measurements. No oscillations are apparent.

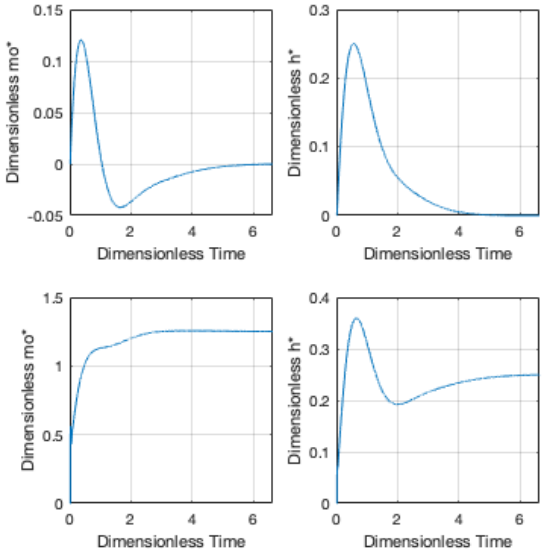

Figure 13. Closed-loop response of a system with 20% off measurements of the mass outflow and, implicitly, height: unity step-change in disturbance M_T (top) and unity step-change in mass outflow M^*_o (bottom).

4 FUTURE WORK

Based on this paper's study of the multiloop PID control of a buffer silo using a height-inferring system to reduce the number of sensors to one, the following future work can be conducted:

The errors associated with measuring the mass outflow and the time delay introduced can be better quantified using a DEM simulation that implements the two PID controllers.

For the PID parameters used for this paper (Table 3), a separate height measurement seemed to actually destabilise the system. A more in-depth comparison between the height-inferring system and a separate height-measuring technique can provide more insight into the advantages (and disadvantages) of the former.

The PID parameters were tuned empirically for the best stability in light of real time delay. More sophisticated tuning techniques can be implemented to analyse their response and check for better stability and speed of response.

5 CONCLUSIONS

This paper developed a mathematical model of a typical buffer silo, treating the granular fluid as a continuous liquid with a discharge coefficient. The proposed control problem was concerned with maintaining the mass outflow $\dot{m}_o$ and height $\dot{h}$ of the granular fluid against fluctuations in the top mass inflow $\dot{m}_T$. This was achieved by controlling the bottom chute position (mass stopped by the chute) $\dot{m}_C$ and the amount of granular fluid diverted from the top inflow by a diverter valve $\dot{m}_D$. The control scheme used a multiloop arrangement of two PID controllers coupled in a 1-1/2-2 manner: controller 1 manipulated the chute by using the mass outflow error signal, while controller 2 manipulated the diverter valve by using the height error signal.

The mass outflow was considered to be measured using a weighing scale underneath the silo with first-order dynamics. It was recognised that the outflow velocity was driven by the potential energy of the granular fluid inside the silo. Therefore, a zero-order approximation of the weighing scale was used to infer the fluid height which also made use of PID signals (depicted in Equation 21).

The stability of the system was first evaluated analytically using the characteristic equation and Nyquist diagrams. It was found that controller 2 is the one that mainly introduces instability in the system. Moreover, the integral gains introduce a lower boundary for the stability region of the proportional gains. These findings were used to empirically tune the two PID controllers for the best robustness.

A Simulink™block model was then developed to simulate the control system. The open-loop response showed the expected self-stabilising nature of the buffer silo. For the closed-loop response, five aspects were analysed:

1. The control system counteracted disturbances very robustly: quick rise time, relatively low peaks and no oscillations. The changes in height were insignificant compared to the height of the fluid, being smaller by three orders.
2. For a step-change in the set mass outflow, the system responded relatively quickly with no overshoot in the mass outflow. For a step-change in the set height, the height response was relatively quick with minimal overshoot. However, the mass outflow showed bigger fluctuations, showcasing the difficulty of controlling the height using the diverter valve.
3. The time delay in the mass outflow measurement system destabilises the system: for increasing time delay, the response becomes more abrupt, then starts exhibiting oscillations, before becoming unstable. However, the settling time does not seem to be affected.
4. The inferred height follows the real height well without much delay. However, for very noisy measurements, the overshoot can become larger- but it is still insignificant compared to the height of a silo. A separate measurement of the height follows it more closely, but, interestingly, destabilises the system.
5. In the case of measurements that are 20% off, the system stability does not seem to be affected. For a step-change in the set mass outflow, the system settles at values that are 25% higher. For the height, this is still insignificant, but may be problematic for the mass outflow.

Overall, the control system proved very robust in handling disturbances, real time delays and off-measurements. The developed height-inferring system was used to successfully predict and control the granular fluid height in the silo.

APPENDIX

The characteristic equation, written explicitly for this model, is:

$$det\left(I_2 - [PID]K_{ep}[FCE]G_P G_m\right) = 0 \tag{27}$$

$$det\left(\begin{bmatrix}1 & 0\\ 0 & 1\end{bmatrix} - \begin{bmatrix}K_{cp1} + K_{ci1}/s + K_{cd1}s & 0\\ 0 & K_{cp2} + K_{ci2}/s + K_{cd2}s\end{bmatrix} \begin{bmatrix}K_{ep1} & 0\\ 0 & K_{ep2}\end{bmatrix} \begin{bmatrix}\frac{K_c}{\tau_c s+1} & 0\\ 0 & \frac{K_d}{\tau_d s+1}\end{bmatrix} \begin{bmatrix}\frac{-\tau_P s}{\tau_P s+1} & \frac{-1}{\tau_P s+1}\\ \frac{K_P}{\tau_P s+1} & \frac{-K_P}{\tau_P s+1}\end{bmatrix} \begin{bmatrix}\frac{K_m}{\tau_m s+1} & 0\\ 0 & \frac{K_h}{\tau_m s+1}\end{bmatrix}\right) = 0 \tag{28}$$

REFERENCES

[1] Coperion. High efficiency product transfer, weighing and dispensing, and extrusion for the bakery and tortilla industries. Retreived from `https://www.coperion.com/en/industries/food-pet-food/flours-starches-bakery-ingredients/`, 2019. Accessed: 2019-02-27.

[2] Sandeep Kumar Sunori, Shweta Shree, and Pradeep Kumar Juneja. Control of sugarcane crushing mill process: A comparative analysis. In *2015 International Conference on Soft Computing Techniques and Implementations (ICSCTI)*. IEEE, October 2015.

[3] Dale E. Seborg, Duncan A. Mellichamp, and Thomas F. Edgar. *Process Dynamics and Control, 4th Edition*. Wiley, 2016.

[4] QI BIAN. Bulk flow properties of wheat. Retreived from `http://citeseerx.ist.psu.edu/viewdoc/download?doi=10.1.1.849.3830&rep=rep1&type=pdf`, 2014. Accessed: 2019-03-25.